Yu *et al. Satellite Navigation* (2023) 4:20
https://doi.org/10.1186/s43020-023-00108-3

Satellite Navigation
https://satellite-navigation.springeropen.com/

ORIGINAL ARTICLE Open Access

A state-domain robust autonomous integrity monitoring with an extrapolation method for single receiver positioning in the presence of slowly growing fault

Zhangjun Yu[1,2], Qiuzhao Zhang[1,2*], Shubi Zhang[1], Nanshan Zheng[1,2] and Keqiang Liu[3]

Abstract

Single receiver positioning has been widely used as a standard and standalone positioning technique for about 25 years. To detect the slowly growing faults caused by satellite and receiver clocks in single receiver positioning, the Autonomous Integrity Monitoring with an Extrapolation method (AIME) was proposed based on the Kalman filter measurement domain. However, AIME was designed with the assumption of there is the same number of visible satellites at each epoch, which limits its application. To address this issue, this paper proposes a state-domain Robust Autonomous Integrity Monitoring with the Extrapolation Method (SRAIME). The slowly growing fault detection statistics is established based on the difference between the estimates of the state propagator and the posterior state estimation in Kalman filtering. Meanwhile, singular value decomposition is adopted to factor the covariance matrix of the difference to increase computational robustness. Besides, the relevant formulas of the proposed method are theoretically derived, and it is proven that the proposed method is suitable for any positioning model based on the Kalman filter. Additionally, the results of two experiments indicate that SRAIME can detect slowly growing faults in single receiver positioning earlier than AIME.

Keywords GNSS, Single receiver positioning, Slow growing fault, State domain, Fault detection

Introduction

In the 1980s, single receiver positioning based on pseudo-range measurements was the mainstream dynamic positioning, while the carrier phase measurements were mainly used for static geodetic surveys. With the further development of the Global Navigation Satellite System (GNSS), the carrier phase-based positioning has been widely used. It is acknowledged that ambiguity resolution is the key to high-precision positioning. Real-Time Kinematic (RTK) technique can quickly fix ambiguity by performing double-difference processing of the observations of the reference station and the rover (Gao et al., 1997; Wanninger, 1995). Compared with the RTK positioning that requires two receivers, Precise Point Positioning (PPP) can achieve high-precision positioning with only one receiver, and also provide high-precision services to the users in the environments and scenarios such as gobi, mining, and offshore, where RTK services are not applicable. The concept and model of PPP were first proposed in 1997 (Zumberge et al., 1997). Meanwhile, a precise data processing software GIPSY was developed with a plane accuracy of 1 cm and an elevation accuracy

*Correspondence:
Qiuzhao Zhang
qiuzhao.zhang@cumt.edu.cn
[1] Jiangsu Key Laboratory of Resources and Environmental Information Engineering, China University of Mining and Technology, Xuzhou 221116, China
[2] School of Environment Science and Spatial Informatics, China University of Mining and Technology, Xuzhou 221116, China
[3] Zhejiang Deqing Zhilu Navigation Research Institute Co.,Ltd., Huzhou 313299, China

of 2 cm. Besides, by combining PPP and RTK, PPP-RTK can achieve fast convergence (Li et al., 2022a, b). It was confirmed that attributed to the reduction of the multipath effect, the application of a survey-grade antenna instead of the patch one can significantly improve the performance of low-cost receiver Single-Frequency Ionospheric-Free Precise Point Positioning (SF-IF PPP) (Paziewski, 2022). Moreover, the PPP technique on smartphones has attracted increasing interest in recent years (Li et al., 2022c; Shinghal et al., 2021), and a Mixed Single- and Dual-frequency Quad-constellation Precise Point Positioning (MSDQ-PPP) model was developed to improve the positioning performance on smartphones by exploiting all available GNSS observations (Li and Cai, 2022). The BeiDou Navigation Satellite System (BDS) has obtained global service capability since the launch of the 55th BeiDou-3 Navigation Satellite System (BDS-3) satellite on June 23, 2020. A model of the multi-frequency kinematic PPP of Global Positioning System (GPS), BeiDou-2 Navigation Satellite System (BDS-2), and BDS-3 based on vehicle-borne data was evaluated to fully utilize BDS-2 + BDS-3 signals (B1I, B2I, B3I, B1C, and B2a) (Bu et al., 2020; Lv et al., 2022).

The Kalman filter plays an important role in GNSS data processing. A basic assumption for the application of standard Kalman filtering is that both the dynamic model and the stochastic information provided to the filter are accurate (Hide et al., 2003). Any deviation from this assumption or the existence of many outlying observations can result in poor performance such as abrupt faults and slowly growing faults in the filtering result (Geng et al., 2008; Wang 2009). Therefore, it is necessary to conduct fault detection to ensure the positioning reliability and precision (Bruggemann et al., 2011; Du et al., 2021; Liu et al., 2016).

In fault detection, the chi-square test methods are the classical ones and have been widely used, because they can detect the faults caused by the outliers in the measurements and inaccurate dynamic models or random information of the Kalman filter. The methods determine the fault detection threshold based on the probability of a False Alarm (FA), so they do not require any user interaction. The Residual Chi-square Test Method (RCTM) detects faults based on the innovation of the Kalman filter (i.e., the measurement prediction error), and it can detect abrupt faults with a small amount of calculation (Zhu et al., 2016; Wang et al., 2020; Wang 2008; Gao et al., 2021; Chen et al., 2021a). However, this method directly assesses the measurement prediction error, but indirectly the filtering state estimate error. In fact, accurate and consistent measurement predictions do not necessarily contribute to accurate and consistent state estimates (Duník et al., 2018). Therefore, the State-domain Robust Chi-square Test Method (SRCTM) was proposed, and its fault detection statistics was based on the difference between the prior and posterior state estimations in the Kalman filter. Both RCTM and SRCTM can detect abrupt faults accurately, and they are equivalent under certain conditions (Yu et al., 2021).

The slowly growing fault was regarded as the worst fault mode (Bhatti et al., 2007a). Slowly growing faults are typical of the GPS and receiver clocks, and the snapshot integrity algorithms like RCTM and SRCTM take a long time to detect these types of faults because they need a lot of time to reach the fault threshold. AIME is a sequential algorithm where the measurements used are not limited to a single epoch, and its fault detection statistics is based on the RCTM (Diesel and King 1995). However, the assumption of the same number of visible satellites at each epoch limits its application, and thus AIME is suitable for simulation-based fault detection, not for real-time fault detection. Similarly, the rate detector algorithms based on the statistics of AIME have the same defect (Bhatti et al., 2007b, 2012). Additionally, AIME and the rate detector algorithms are all based on the innovation of the Kalman filter, indicating that they directly assess the measurement prediction error, but indirectly the filtering state estimate error (Duník et al., 2018).

To overcome the aforementioned limitations, this paper proposes a state-domain robust autonomous integrity monitoring with an extrapolation method, which directly works in the state domain, is suitable for any positioning model based on the Kalman filter, and can detect the slowly growing fault earlier.

The rest of this paper is organized as follows. In "The dynamic and observation equations of the single receiver positioning" Section lists the formulas of the dynamic and observation equations of the single receiver positioning. In "Problem formulation" Section, the effect of a slowly growing fault is evaluated, and AIME is reviewed and analysed. Then, SRAIME is derived and described in "Kalman filter for single receiver positioning" Section. In "Effect of a slowly growing fault" Section, the experiments and its analysis are presented. Finally, the paper is concluded in "Autonomous integrity monitoring with the extrapolation method" Section.

The dynamic and observation equations of the single receiver positioning

In this section, an overview of single receiver positioning models including classical Single Point Positioning (SPP) and PPP is provided, and the formulation of the measurements used in each positioning model is described in detail.

The pseudo-range observation equation of SPP can be expressed as:

$$P = \rho - c\delta t + I + T + \varepsilon \tag{1}$$

where P is the pseudo-range measurement, ρ is the true geometric range between the receiver and the satellite, $c\delta t$ is the receiver clock offset scaled by the speed of light, I is the ionospheric delay, T is the troposphere delay, and ε represents the unmodelled and residual errors.

The measurement model of SPP is established by Eq. (1) after a linearization at the approximate coordinates of the station:

$$P - \rho_0 - D = ldX + mdY + ndZ + c\delta t \tag{2}$$

where ρ_0 is the approximate distance between the receiver and the satellite, $D = I + T + \varepsilon$, (l, m, n) are direction cosines, and $(\mathrm{d}X, \mathrm{d}Y, \mathrm{d}Z)$ represents the receiver coordinate correction (Gaglione et al., 2015).

In the same way, the pseudo-range observation equation and the carrier phase observation equation of PPP are expressed as:

$$P = \rho - c\delta t + I + T + M_{wet} dD_w + \varepsilon(P) \tag{3}$$

$$L = \rho - c\delta t - I + T + M_{wet} dD_w + \lambda N + \varepsilon(L) \tag{4}$$

where M_{wet} is the tropospheric wet delay mapping function, $\mathrm{d}D_{\mathrm{w}}$ is the tropospheric zenith wet delay correction parameter, $\varepsilon(P)$ represents the unmodelled and residual errors of the pseudo-range observation; L is the carrier phase measurement, λ is the wavelength of the carrier, N is the phase ambiguity term (in cycles), and $\varepsilon(L)$ represents the unmodelled and residual errors of the carrier phase observation.

The measurement model of PPP is established from Eqs. (3) and (4) after a linearization at the approximate coordinates of the station:

$$P - \rho_0 - D_P = ldX + mdY + ndZ + c\delta t + M_{wet} dD_w \tag{5}$$

$$L - \rho_0 - D_L = ldX + mdY + ndZ + c\delta t + M_{wet} dD_w \tag{6}$$

where $D_P = I + T + \varepsilon(P)$, $D_L = T - I + \varepsilon(L)$ (Sanz et al., 2013).

Combining (2), (5), and (6), the dynamic and observation equations of the single receiver positioning can be simplified as:

$$\boldsymbol{x}_{k+1} = \boldsymbol{f}_k(\mathbf{x}_k) + \mathbf{w}_k \tag{7}$$

$$\mathbf{z}_k = \boldsymbol{h}_{\mathbf{k}}(\mathbf{x}_{\mathbf{k}}) + \mathbf{v}_k \tag{8}$$

where $\mathbf{x}_k$ represents the state of the system, including the receiver coordinate corrections, clock error corrections, tropospheric zenith wet delay correction, and ambiguity parameters; $\boldsymbol{f}_k$ is the system function, $\mathbf{w}_k$ is the system noise vector and is usually assumed to be zero-mean Gaussian white noise with a covariance matrix $\boldsymbol{Q}_k$; $\boldsymbol{z}_k$ represents the measurements in Eqs. (2), (5) and (6), $\boldsymbol{h}_k$ is the measurement function, and $\mathbf{v}_k$ is the measurement noise vector, which is commonly assumed to be zero-mean Gaussian white noise with a covariance matrix $\boldsymbol{R}_k$ (Yu et al., 2021).

Problem formulation

The problem of slowly growing fault detection was thoroughly investigated over the past decades. In this section, the Kalman filter for single receiver positioning and the effect of slowly growing fault are formulated; meanwhile, the AIME, which is a popular test used for several decades, is introduced and analysed.

Kalman filter for single receiver positioning

The methods designed for slowly growing fault detection in the single receiver positioning are based on the Gaussian assumption and statistical hypothesis testing. Consider a state variable $\mathbf{x}$ with a known prior Gaussian Probability Density Function (PDF)

$$p(\mathbf{x}) = \mathcal{N}\{\mathbf{x}; \hat{\mathbf{x}}', \boldsymbol{P}'_{xx}\} \tag{9}$$

where $\mathcal{N}\{\mathbf{x}; \hat{\mathbf{x}}', \boldsymbol{P}'_{xx}\}$ represents the normal distribution with the mean $\hat{\mathbf{x}}' = E[\boldsymbol{x}]$ and the covariance matrix $\boldsymbol{P}'_{xx} = \mathrm{cov}[\boldsymbol{x}]$; meanwhile, the time update and measurement update of the Kalman filter for single receiver positioning can be represented as:

$$\hat{\mathbf{x}}_k = \hat{\mathbf{x}}'_k + \boldsymbol{K}_k(\mathbf{z}_k - \hat{\mathbf{z}}'_k) \tag{10}$$

$$\boldsymbol{K}_k = \mathbf{P}'_{xz,k}(\mathbf{P}'_{zz,k})^{-1} \tag{11}$$

$$\mathbf{P}_{xx,k} = \mathbf{P}'_{xx,k} - K_k \mathbf{P}'_{zz,k}(K_k)^T \tag{12}$$

$$\hat{\mathbf{x}}'_{k+1} \approx \int \boldsymbol{f}_k(\mathbf{x}_k)\mathcal{N}\{\mathbf{x}_k; \hat{\mathbf{x}}_k, \boldsymbol{P}_{xx,k}\}d\mathbf{x}_k \tag{13}$$

$$\mathbf{P}'_{xx,k+1} \approx \int (\boldsymbol{f}_k(\mathbf{x}_k) - \hat{\mathbf{x}}'_{k+1})(\boldsymbol{f}_k(\mathbf{x}_k) - \hat{\mathbf{x}}'_{k+1})^{\mathrm{T}} \mathcal{N}\{\mathbf{x}_k; \hat{\mathbf{x}}_k, \boldsymbol{P}_{xx,k}\}d\mathbf{x}_k + \mathbf{Q}_k \tag{14}$$

$$\hat{\mathbf{z}}'_k \approx \int h_k(\mathbf{x}_k)\boldsymbol{\mathcal{N}}\{\mathbf{x}_k; \hat{\mathbf{x}}'_k, \mathbf{P}'_{xx,k}\}d\mathbf{x}_k \tag{15}$$

$$\mathbf{P}'_{zz,k} \approx \int (h_k(\mathbf{x}_k) - \hat{\mathbf{z}}'_k)(h_k(\mathbf{x}_k) - \hat{\mathbf{z}}'_k)^{\mathrm{T}} \mathcal{N}\{\mathbf{x}_k; \hat{\mathbf{x}}'_k, \mathbf{P}'_{xx,k}\} d\mathbf{x}_k + \mathbf{R}_k \tag{16}$$

$$\mathbf{P}'_{xz,k} \approx \int (\mathbf{x}_k - \hat{\mathbf{x}}'_k)(h_k(\mathbf{x}_k) - \hat{\mathbf{z}}'_k)^{\mathrm{T}} \mathcal{N}\{\mathbf{x}_k;'_k, \mathbf{P}'_{xx,k}\} d\mathbf{x}_k \tag{17}$$

where $\hat{\mathbf{x}}'_k$ is the prior state estimate, $\mathbf{P}'_{xx,k}$ is the covariance matrix of $\hat{\mathbf{x}}'_k$, $\boldsymbol{K}_k$ is the gain matrix, $\hat{\mathbf{x}}_k$ is the posterior state estimate, $\mathbf{P}_{xx,k}$ is the covariance matrix of $\hat{\mathbf{x}}'_k$, $\hat{\mathbf{z}}'_k$ is the predictive measurement, $\mathbf{P}'_{zz,k}$ is the covariance matrix of $\hat{\mathbf{z}}'_k$, and $\mathbf{P}'_{xz,k}$ denotes the "cross-covariance" matrix of joint $\hat{\mathbf{x}}'_k$ and $\hat{\mathbf{z}}'_k$.

Effect of a slowly growing fault

In principle, a fault can be detected by using statistical hypothesis testing. The null hypothesis H_0: assuming no fault, i.e., assuming $\hat{\mathbf{x}}_k$ and $\mathbf{P}_{xx,k}$ are accurate enough, is tested against the alternative hypothesis H_1, i.e., assuming there is a fault. Generally, faults can be divided into two groups:

Abrupt fault, with relatively small detection difficulty. The current measurement value or state value-based methods such as RCTM and SRCTM have less calculation amount and are extremely effective. The fault detection statistics at the time of fault occurrence is greater than the fault detection threshold.

Slowly growing fault, which is more difficult to detect than abrupt fault, because the residual at each epoch is very small. The slowly growing fault at k epoch can be expressed as $\boldsymbol{S}_k$, and the cumulative error of the slowly growing fault in $\hat{\mathbf{x}}_k$ can be expressed as $\boldsymbol{A}_k$:

$$\hat{\mathbf{x}}_{\mathrm{S},k} = \hat{\mathbf{x}}_k + \boldsymbol{A}_k \tag{18}$$

$$\mathbf{z}_{\mathrm{S},k} = \mathbf{z}_k + \boldsymbol{S}_k \tag{19}$$

where subscript $\otimes_{\mathrm{S},k}$ represents a vector containing a slowly growing fault (assume $\boldsymbol{S}_k > \mathbf{0}$, $\boldsymbol{A}_k > \mathbf{0}$). When using a snapshot method such as RCTM for fault detection, in theory, the innovation including fault at k epoch is:

$$\boldsymbol{e}_{\mathrm{S},k+1} = \mathbf{z}_{\mathrm{S},k+1} - \hat{\mathbf{z}}'_{k+1} = \boldsymbol{e}_{k+1} + \boldsymbol{S}_{k+1} \tag{20}$$

$$\boldsymbol{e}_{k+1} = \mathbf{z}_{k+1} - \hat{\mathbf{z}}'_{k+1} \tag{21}$$

However, considering the cumulative error $\boldsymbol{A}_k$, the innovation including fault is:

$$\boldsymbol{e}_{\mathrm{S},k+1} = \mathbf{z}_{\mathrm{S},k+1} - \hat{\mathbf{z}}'_{\mathrm{S},k+1} < \boldsymbol{e}_{k+1} + \boldsymbol{S}_{k+1} \tag{22}$$

due to

$$\begin{aligned} \hat{\mathbf{z}}'_{\mathrm{S},k+1} &= \int \boldsymbol{h}_{k+1}(\mathbf{x}_{k+1}) \mathcal{N}\{\mathbf{x}_{k+1}; \hat{\mathbf{x}}'_{\mathrm{S},k+1}, \boldsymbol{P}'_{xx,k+1}\} \mathrm{d}\mathbf{x}_{k+1} \\ &> \int \boldsymbol{h}_{k+1}(\mathbf{x}_{k+1}) \mathcal{N}\{\mathbf{x}_{k+1}; \hat{\mathbf{x}}'_{k+1}, \boldsymbol{P}'_{xx,k+1}\} \mathrm{d}\mathbf{x}_{k+1} = \hat{\mathbf{z}}'_{k+1} \end{aligned} \tag{23}$$

$$\hat{x}'_{\mathrm{S},k+1} \approx \int f_k(\mathbf{x}_k) \mathcal{N}\{\mathbf{x}_k; \hat{\mathbf{x}}_{\mathrm{S},k}, \boldsymbol{P}_{xx,k}\} d\mathbf{x}_k > \int f_k(\mathbf{x}_k) \mathcal{N}\{\mathbf{x}_k; \hat{x}_k, \boldsymbol{P}_{xx,k}\} d\mathbf{x}_k = \hat{x}'_{k+1} \tag{24}$$

It can be seen that the overall error of the slowly growing fault increases with time, while the residual in (22) is less than its theoretical value. As a result, the fault detection statistics of RCTM and SRCTM are always less than the fault detection threshold. Therefore, it is necessary to employ the sequential algorithm to amplify the slowly growing fault at each epoch in fault detection.

Autonomous integrity monitoring with the extrapolation method

This section describes the autonomous integrity monitoring with the extrapolation method which detects slowly growing faults using the innovation of the Kalman filter:

Step 1: Define a required (or allowed) probability of false alert P_{FA}.

Step 2: Define the extrapolation cycle m. If $k \leq m$, then detect the faults using RCTM; otherwise, take $\hat{\mathbf{x}}_{k-m}$ in (10) and $\mathbf{P}_{xx,k-m}$ in (12) as the extrapolated initial state $p(\mathbf{x}_{k-m}^{\mathrm{SP}}) = \mathcal{N}\left\{\mathbf{x}_{k-m}^{\mathrm{SP}}; \hat{\mathbf{x}}_{k-m}^{\mathrm{SP}}, \mathbf{P}'^{\mathrm{SP}}_{xx,k-m}\right\}$, and perform time update to the k epoch by the state propagator:

$$\hat{\mathbf{x}}_{k-m+i}^{\mathrm{SP}} \approx \int \boldsymbol{f}_{k-m+i-1}(\mathbf{x}_{k-m+i-1}^{\mathrm{SP}}) \mathcal{N}\left\{\mathbf{x}_{k-m+i-1}^{\mathrm{SP}}; \hat{\mathbf{x}}_{k-m+i-1}^{\mathrm{SP}}, \mathbf{P}'^{\mathrm{SP}}_{xx,k-m+i-1}\right\} \mathrm{d}\mathbf{x}_{k-m+i-1}^{\mathrm{SP}} \tag{25}$$

$$\boldsymbol{P}'^{\mathrm{SP}}_{xx,k-m+i} \approx \int (\boldsymbol{f}_{k-m+i-1}(\mathbf{x}_{k-m+i-1}^{\mathrm{SP}}) - \hat{\mathbf{x}}_{k-m+i}^{\mathrm{SP}}) \left(\boldsymbol{f}_{k-m+i-1}(\mathbf{x}_{k-m+i-1}^{\mathrm{SP}}) - \hat{\mathbf{x}}_{k-m+i}^{\mathrm{SP}}\right)^{\mathrm{T}} \cdot \boldsymbol{\mathcal{N}}\left\{\mathbf{x}_{k-m+i-1}^{\mathrm{SP}}; \hat{\mathbf{x}}_{k-m+i-1}^{\mathrm{SP}}, \boldsymbol{P}'^{\mathrm{SP}}_{xx,k-m+i-1}\right\} \mathrm{d}\mathbf{x}_{k-m+i-1}^{\mathrm{SP}} + \mathbf{Q}_{k-m+i-1} \tag{26}$$

where $\hat{\mathbf{x}}_{k-m+i}^{\mathrm{SP}}$ is the prior state estimate of the state propagator, $\boldsymbol{x}_{k-m+i}^{\mathrm{SP}}$ is the state of the state propagator, $\mathbf{P}'^{\mathrm{SP}}_{xx,k-m+i}$ is the covariance matrix of $\hat{\mathbf{x}}_{k-m+i}^{\mathrm{SP}}$, and $1 \leq i \leq m$. Step 3: Calculate $\boldsymbol{e}_{k-m+i}^{\mathrm{SP}}$ and its covariance matrix $\mathbf{P}'^{\mathrm{SP}}_{zz,k-m+i}$:

$$\boldsymbol{e}_{k-m+i}^{\mathrm{SP}} = \boldsymbol{z}_{k-m+i} - \hat{\boldsymbol{z}}'^{\mathrm{SP}}_{k-m+i} \tag{27}$$

$$\boldsymbol{P}'^{\mathrm{SP}}_{zz,k-m+i} \approx \int (\boldsymbol{h}_{k-m+i}(\mathbf{x}_{k-m+i}^{\mathrm{SP}}) - \hat{\boldsymbol{z}}'^{\mathrm{SP}}_{k-m+i})(\boldsymbol{h}_{k-m+i}(\mathbf{x}_{k-m+i}^{\mathrm{SP}}) - \hat{\boldsymbol{z}}'^{\mathrm{SP}}_{k-m+i})^{\mathrm{T}} \cdot \boldsymbol{\mathcal{N}}\left\{\mathbf{x}_{k-m+i}^{\mathrm{SP}}; \hat{\mathbf{x}}_{k-m+i}^{\mathrm{SP}}, \mathbf{P}'^{\mathrm{SP}}_{xx,k-m+i}\right\} \mathrm{d}\mathbf{x}_{k-m+i}^{\mathrm{SP}} + \mathbf{R}_{k-m+i} \tag{28}$$

where $\hat{\mathbf{z}}'^{\mathrm{SP}}_{k-m+i}$ is the predictive measurement of the state propagator:

$$\hat{\boldsymbol{z}}'^{\mathrm{SP}}_{k-m+i} \approx \int \boldsymbol{h}_{k-m+i}(\mathbf{x}_{k-m+i}^{\mathrm{SP}}) \mathcal{N}\left\{\mathbf{x}_{k-m+i}^{\mathrm{SP}}; \hat{\mathbf{x}}_{k-m+i}^{\mathrm{SP}}, \mathbf{P}'^{\mathrm{SP}}_{xx,k-m+i}\right\} \mathrm{d}\mathbf{x}_{k-m+i}^{\mathrm{SP}} \tag{29}$$

Step 4: Calculate AIME fault detection statistics:

$$\alpha_{\mathrm{avg},k} = (\boldsymbol{e}_{\mathrm{avg},k})^{\mathrm{T}} (\mathbf{P}_{zz,\mathrm{avg},k})^{-1} \boldsymbol{e}_{\mathrm{avg},k}, \alpha_{\mathrm{avg},k} \sim p(\alpha_{\mathrm{avg},k}) \tag{30}$$

$$\mathbf{P}_{zz,\mathrm{avg},k}^{-1} = \sum_{i=1}^{m} (\mathbf{P}'^{\mathrm{SP}}_{zz,k-m+i})^{-1} \tag{31}$$

$$\boldsymbol{e}_{\mathrm{avg},k} = (\mathbf{P}_{zz,\mathrm{avg},k}^{-1})^{-1} \sum_{i=1}^{m} (\mathbf{P}'^{\mathrm{SP}}_{zz,k-m+i})^{-1} \boldsymbol{e}_{k-m+i}^{\mathrm{SP}} \tag{32}$$

If the null hypothesis H_0 is valid, then the PDF $p(\alpha_{\mathrm{avg},k})$ is (approximately) a chi-squared distribution with n_z Degrees of Freedom (DOF), where n_z is the dimension of the measurement domain.

Step 5: Calculate the corresponding P_{FA} quantile

$$q_{\mathrm{FA},k}^{\alpha} = \inf\left\{\alpha_{\mathrm{avg},k} \in: (1 - P_{\mathrm{FA}}) \leq F(\alpha_{\mathrm{avg},k})\right\} \tag{33}$$

where $F(\alpha_{\mathrm{avg},k})$ is the cumulative distribution function with respect to $p(\alpha_{\mathrm{avg},k})$ and the operator inf represents the infimum. The quantile $q_{\mathrm{FA},k}^{\alpha}$ is further denoted as the fault detection threshold.

Step 6: Compare the statistics $\alpha_{\mathrm{avg},k}$ in (30) with the threshold $q_{\mathrm{FA},k}^{\alpha}$ in (33). If $\alpha_{\mathrm{avg},k} \leq q_{\mathrm{FA},k}^{\alpha}$, then it is considered to be no fault; otherwise, it is considered to have a fault.

However, this method directly assesses the measurement prediction error $\mathbf{e}_k$ but indirectly the filtering state estimate error. In fact, accurate and consistent measurement predictions do not necessarily lead to accurate and consistent state estimates (Duník et al., 2018). Besides, the addition and subtraction of $\mathbf{P}'^{\mathrm{SP}}_{zz,k-m+i}$ at different epochs in (31) require the same number of visible satellites at each epoch, while the number of visible satellites changes in real-time dynamic single-point positioning.

State-domain robust autonomous integrity monitoring with the extrapolation method

In this section, the State-domain Robust Autonomous Integrity Monitoring with the Extrapolation method (SRAIME) is proposed and described.

This method is developed based on SRCTM, and its statistical properties are summarized below:

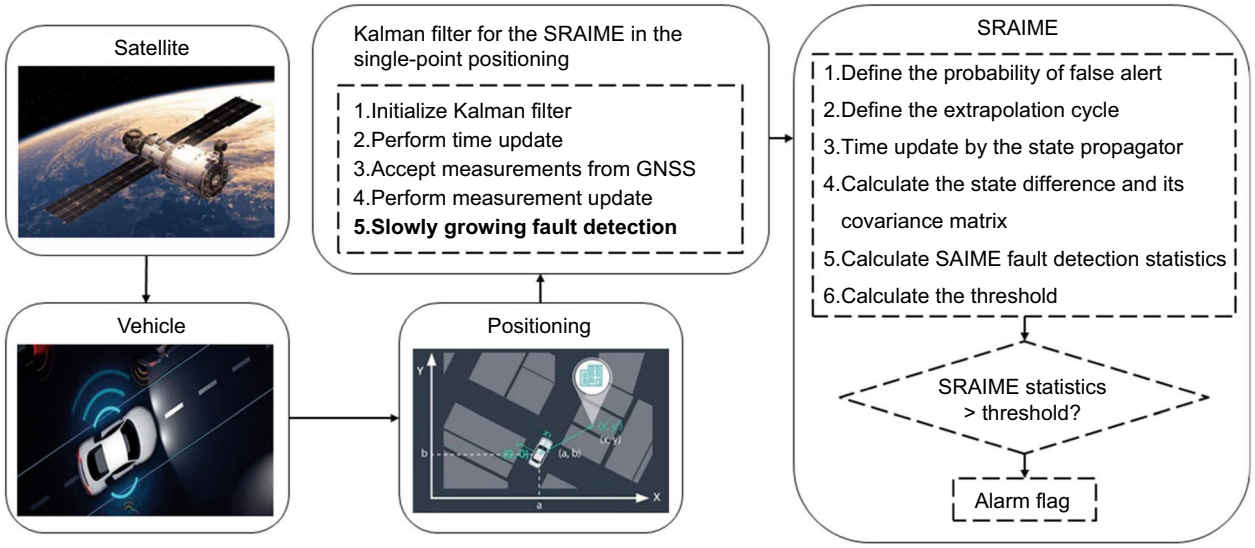

Fig. 1 The flowchart of the SRAIME

$$\mathbf{d}_k = \hat{\mathbf{x}}_k - \hat{\mathbf{x}}'_k \tag{34}$$

$$\hat{\mathbf{d}}_k = E[\mathbf{d}_k] = \mathbf{0} \tag{35}$$

$$\mathbf{P}_{dd,k} = \mathbf{P}'_{xx,k} - \mathbf{P}_{xx,k} = \boldsymbol{K}_k \mathbf{P}'_{zz,k} (\boldsymbol{K}_k)^{\mathrm{T}} \tag{36}$$

where $\mathbf{d}_k$ is the difference between the prior (13) and posterior state estimates (10), n_x is the dimension of $\mathbf{d}_k$, and $\mathbf{P}_{dd,k}$ is the covariance matrix of $\mathbf{d}_k$ (Yu et al., 2021).

Based on the above introduction, the specific steps of the state-domain robust autonomous integrity monitoring with the extrapolation method are as follows:

Step 1: Define a required (or allowed) probability of false alert P_{FA}.

Step 2: Define the extrapolation cycle m. If $k \le m$, then use SRCTM to detect the faults; otherwise, take $\hat{\mathbf{x}}_{k-m}$ in (10) and $\mathbf{P}_{xx,k-m}$ in (12) as the extrapolated initial state $p(\mathbf{x}^{\mathrm{SP}}_{k-m}) = \mathcal{N}\left\{\mathbf{x}^{\mathrm{SP}}_{k-m}; \hat{\mathbf{x}}^{\mathrm{SP}}_{k-m}, \mathbf{P}'^{\mathrm{SP}}_{xx,k-m}\right\}$, and perform time update to the k epoch by the state propagator in (18) and (19).

Step 3: Calculate $\boldsymbol{d}^{\mathrm{SP}}_{k-m+i}$ and its covariance matrix $\mathbf{P}^{\mathrm{SP}}_{dd,k-m+i}, 1 \le i \le m$:

$$\mathbf{d}^{\mathrm{SP}}_{k-m+i} = \hat{\mathbf{x}}_{k-m+i} - \hat{\mathbf{x}}^{\mathrm{SP}}_{k-m+i} \tag{37}$$

$$\mathbf{P}^{\mathrm{SP}}_{dd,k-m+i} = \mathbf{P}'^{\mathrm{SP}}_{xx,k-m+i} - \mathbf{P}_{xx,k-m+i} \tag{38}$$

Step 4: Calculate SAIME fault detection statistics:

$$\beta_{\mathrm{avg},k} = (\mathbf{d}_{\mathrm{avg},k})^{\mathrm{T}} (\mathbf{P}_{dd,\mathrm{avg},k})^{-1} \mathbf{d}_{\mathrm{avg},k}, \beta_{\mathrm{avg},k} \sim p(\beta_{\mathrm{avg},k}) \tag{39}$$

$$\mathbf{P}^{-1}_{dd,\mathrm{avg},k} = \sum_{i=1}^{m} (\mathbf{P}^{\mathrm{SP}}_{dd,k-m+i})^{-1} \tag{40}$$

$$\mathbf{d}_{\mathrm{avg},k} = (\mathbf{P}^{-1}_{dd,\mathrm{avg},k})^{-1} \sum_{i=1}^{m} (\mathbf{P}^{\mathrm{SP}}_{dd,k-m+i})^{-1} \mathbf{d}^{\mathrm{SP}}_{k-m+i} \tag{41}$$

If the null hypothesis H_0 is valid, then the PDF $p(\beta_{\mathrm{avg},k})$ is (approximately) a chi-squared distribution with n_x DOF.

Step 5: Calculate the corresponding P_{FA} quantile:

$$q^{\beta}_{\mathrm{FA},k} = \inf\left\{\beta_{\mathrm{avg},k} \in: (1 - P_{\mathrm{FA}}) \le F(\beta_{\mathrm{avg},k})\right\} \tag{42}$$

Step 6: Compare the statistics $\beta_{\mathrm{avg},k}$ in (39) with the threshold $q^{\beta}_{\mathrm{FA},k}$ in (42). If $\beta_{\mathrm{avg},k} \le q^{\beta}_{\mathrm{FA},k}$, then it is considered to be no fault; otherwise, it is considered to have a fault.

The flowchart of the practical implementation of the SRAIME is shown in Fig. 1. Although SRAIME also involves the addition and subtraction of $\mathbf{P}^{\mathrm{SP}}_{dd,k-m+i}$ at different epochs, the dimension of $\mathbf{x}_k$ in (7) is a constant, so it is suitable for any positioning model based on the Kalman filter in the presence of slowly growing fault.

Experiments

In this section, the proposed method SRAIME is compared with the Autonomous Integrity Monitoring with the Extrapolation method (AIME) and the snapshot integrity algorithms (including RCTM and SRCTM), and it is verified by single receiver positioning using simulation data and real data. To compare the efficiency of these methods, the probability of false alert P_{FA} is set to

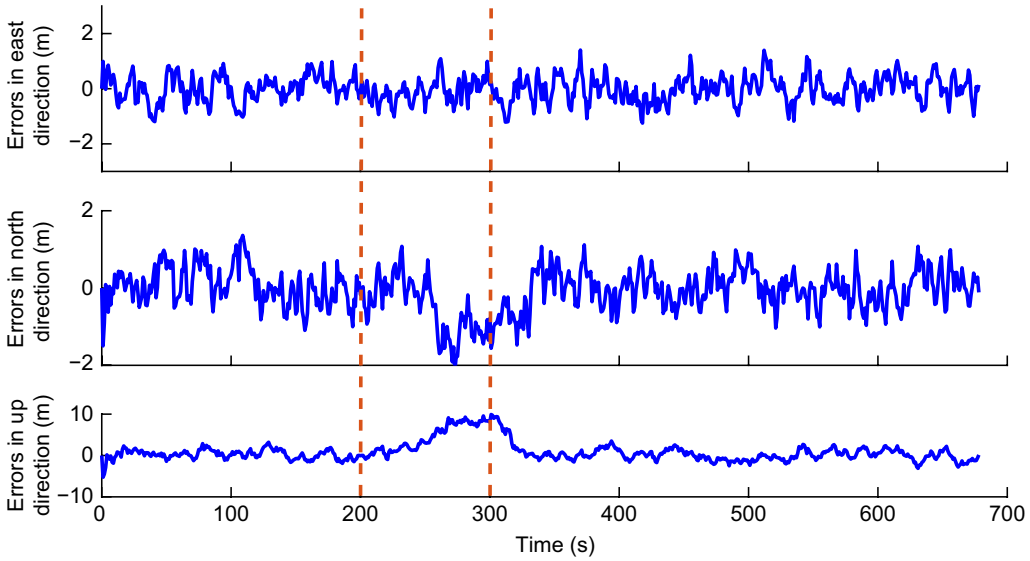

Fig. 2 The position error of the SPP

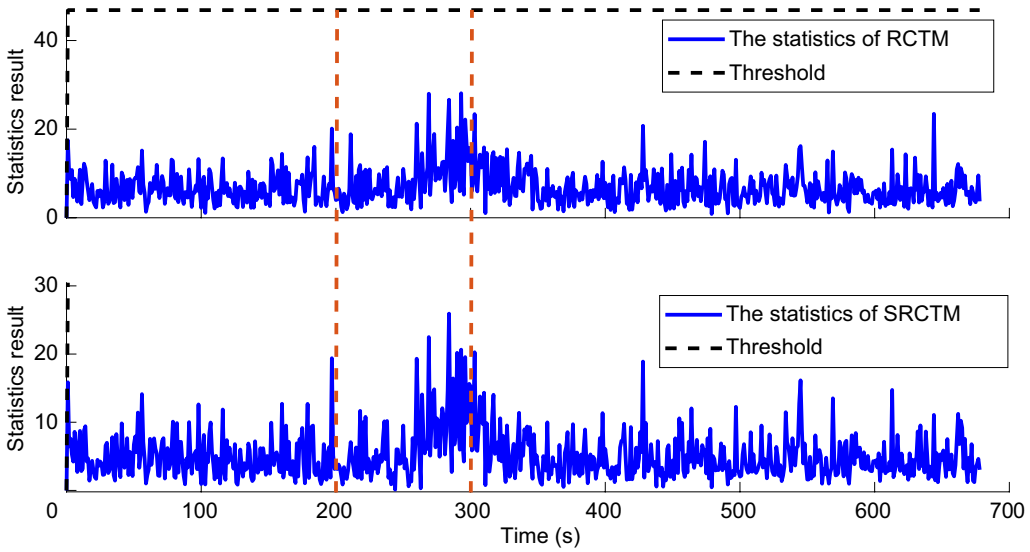

Fig. 3 The statistics of RCTM and SRCTM in the SPP experiment

1×10^{-6}. Meanwhile, the same hardware and software are adopted. The hardware is a personal computer with an Intel Core i5-10,500 CPU and 16 GB main memory. MATLAB R2019b running on a Windows 10 system is used to implement these algorithms.

SPP experiment using simulation data

The dynamic single receiver positioning experiment uses an improved version of the GPSoft toolbox to generate GPS single-frequency pseudo-range observations with a standard deviation of 1 m and pseudo-range increments with a standard deviation of 0.1 m/s (Cox, 1978). As a simulation experiment, the reference trajectory is directly derived from the mathematical model designed in advance. The update frequency of the receiver is 1 Hz. The dimension of the measurement domain is related to the number of visible satellites and is set to a constant of 10. The $\boldsymbol{d}^{\mathrm{SP}}_{k-m+i}$ of SRAIME in (36) only contains the position information of the filtering result, so its dimension is 3. Besides, the extrapolation cycle of AIME and SRAIME is 5 s.

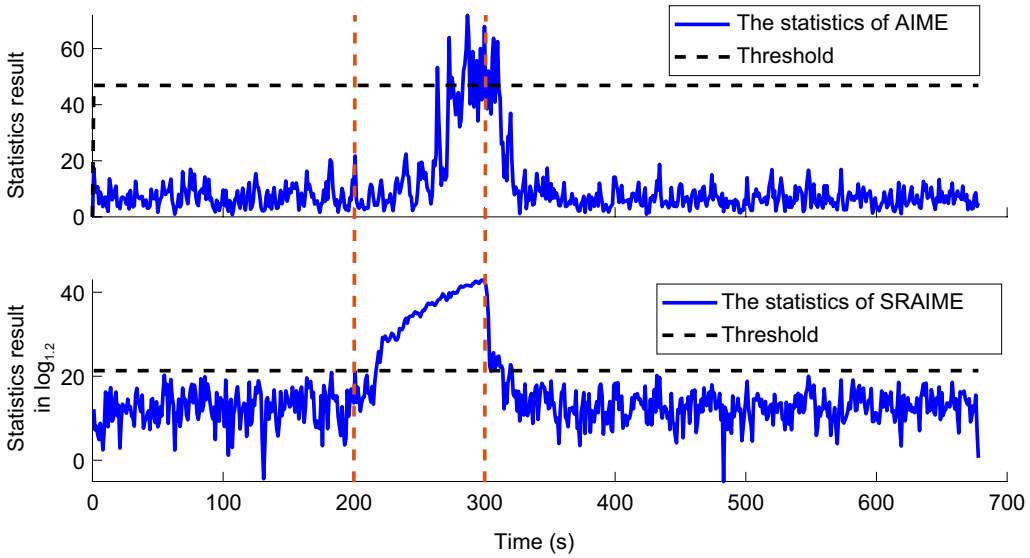

Fig. 4 The statistics of AIME and SRAIME in the SPP experiment

Table 1 The alarm time series of different algorithms in the SPP experiment

Slowly growing fault	Time (s)	Algorithm	Alarm time series (s)
Starting epoch	200	RCTM	-
		SRCTM	-
Ending epoch	300	AIME	264–310
		SRAIME	216–314

Table 2 The data processing strategy of PPP

Items	Strategies
GNSS system	GPS and GLObal NAvigation Satellite System (GLONASS)
Observational model	Ionospheric-Free (IF) combination
Elevation mask	10°
Observation weight	Elevation-dependent weight model
Satellite antenna phase center	Corrected by igs14.atx
Receiver antenna phase center	Corrected by igs14.atx
Ambiguity resolution	No

To verify the effectiveness of SRAIME and compare it with other algorithms, a slowly growing fault $0.001 \times (k - 200)$ ns/s is added to the receiver clock drift artificially from 200 to 300 s. Note that the position error caused by the growth rate is far less than the corresponding triple STandard Deviation (STD).

Figure 2 presents the position error of the SPP. One can see that the slowly growing fault imposed on the receiver clock drift is mainly demonstrated in the up direction.

Figure 3 shows the statistics of RCTM and SRCTM. Both RCTM and SRCTM fail to detect the slowly growing fault. The statistics of AIME and the logarithm of the statistics of SRAIME to the base 1.2 are presented in Fig. 4. It can be observed that the statistics of SRAIME increase rapidly with the slowly growing fault, while that of AIME increase slowly.

Table 1 lists the alarm time series of different algorithms to illustrate the slowly growing fault detection performance of SRAIME in the SPP experiment. The first alarm time of SRAIME is 48 s ahead of that of AIME. This is because SRAIME directly works in the state domain and the slowly growing fault was added in the state domain. Based on the innovation of the Kalman filter, AIME directly assesses the measurement prediction error, but indirectly the filtering state estimate error.

PPP experiment using real data

The dynamic precise point positioning experiment uses the PPP mode in the open-source software GINav to process the data collected at CUMT in March 2019 (Chen et al., 2021b). Table 2 lists the specific processing strategies used in PPP. The update frequency of the receiver is 1 Hz, and the reference solutions were obtained from the NovAtel Inertial Explorer 8.6 software in the smoothed RTK/INS tightly coupled mode. The vehicle and the equipment used are shown in Fig. 5. The dimension of the measurement domain is related to the number of visible satellites. The $\boldsymbol{d}^{\mathrm{SP}}_{k-m+i}$ of

Fig. 5 The GNSS/INS equipment and the van used to collect real data

Fig. 6 The reference trajectory of the PPP experiment

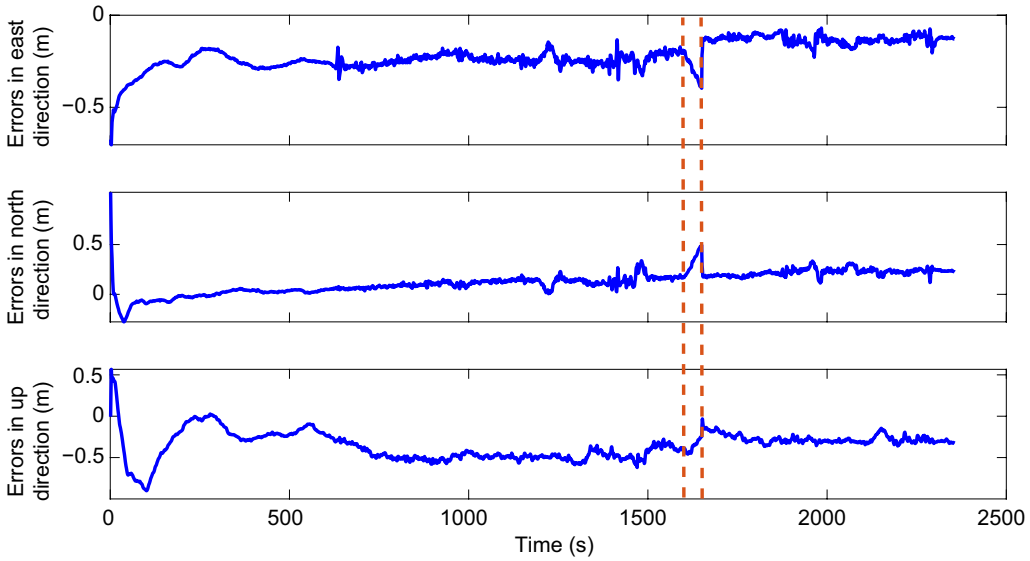

Fig. 7 The position error of the PPP

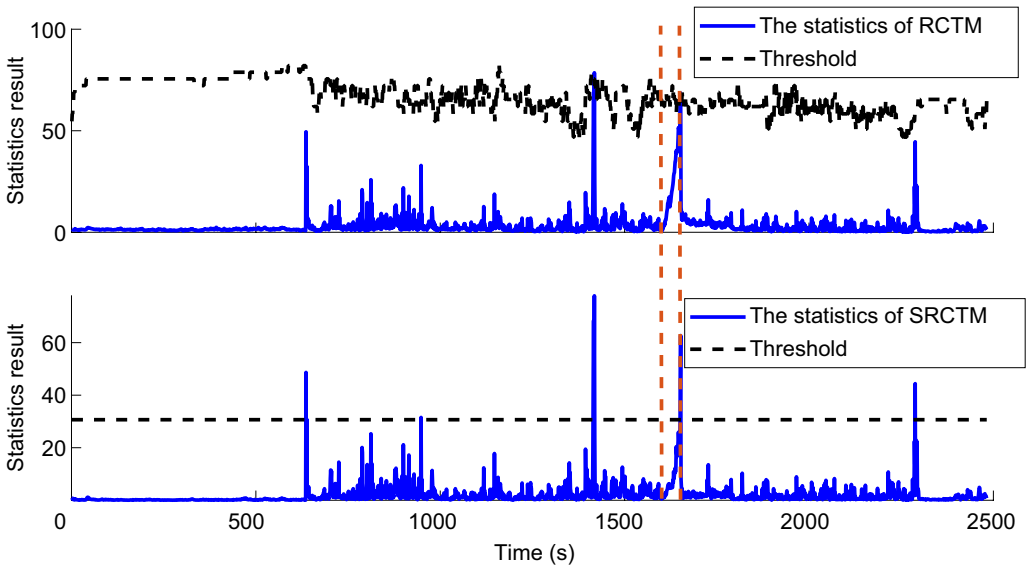

Fig. 8 The statistics of RCTM and SRCTM in the PPP experiment

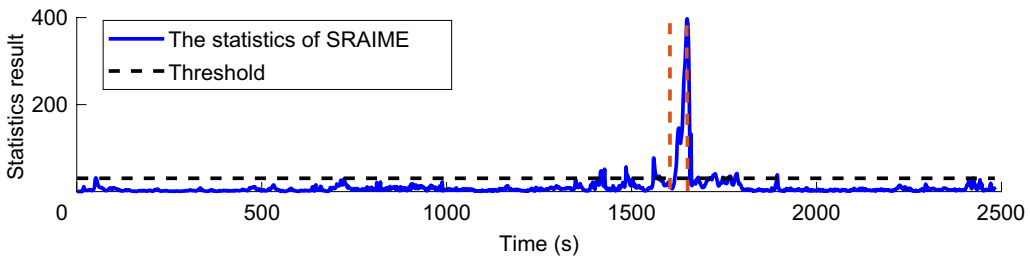

Fig. 9 The statistics of SRAIME in the PPP experiment

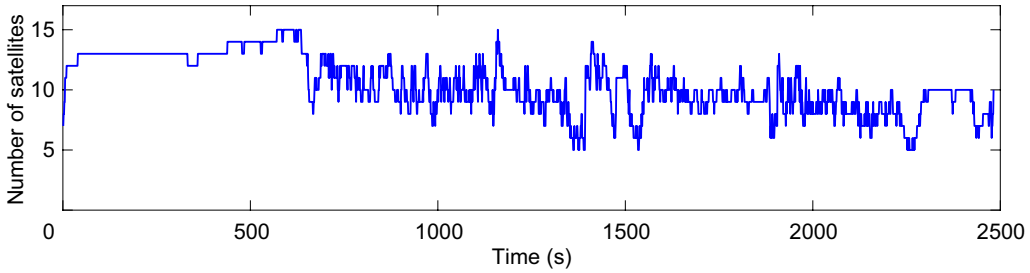

Fig. 10 The number of satellites in the PPP experiment

Table 3 The alarm time series of different algorithms in the PPP experiment

Slowly growing fault	Time (s)	Algorithm	Alarm time series (s)
Starting epoch	1 600	RCTM	1 651
		SRCTM	1 651
Ending epoch	1 650	AIME	-
		SRAIME	1 617–1 660

SRAIME in (36) only contains the position information of the filtering result, so its dimension is 3. Besides, the extrapolation cycle is 10 s.

To verify the effectiveness of SRAIME and compare it with other algorithms, a slowly growing fault $0.01 \times (k - 1600)$ m is added to a carrier phase observation artificially from 1600 to 1650 s. Note that the position error caused by the growth rate is far less than the corresponding 3STDs. Figure 6 shows the reference trajectory of the PPP experiment.

Figure 7 presents the position error of the PPP, and the slowly growing fault imposed on the carrier phase observation is demonstrated in the east, north, and up directions.

Figure 8 shows the statistics of RCTM and SRCTM. Both RCTM and the SRCTM fail to detect the slowly growing fault early. The statistics of SRAIME are illustrated in Fig. 9. One can see that the statistics of SRAIME increase rapidly with the slowly growing fault. Figure 10 shows the number of visible satellites in the PPP experiment. The number of satellites changes in real-time dynamic single point positioning, so AIME is not available in this experiment.

Table 3 shows the alarm time series of different algorithms to illustrate the slowly growing fault detection performance of SRAIME in the PPP experiment. The first alarm time of SRAIM is 34 s ahead that of the snapshot integrity algorithms. The results with different algorithms suggest that SRAIME is suitable for any positioning model based on the Kalman filter, while AIME is designed with the assumption of same number of visible satellites at each epoch and is thus suitable for simulation-based fault detection, not for real-time fault detection.

Conclusions

This paper focuses on detecting the slowly growing fault in single receiver positioning and proposes the SRAIME. The effect of the slowly growing fault and the properties of the proposed method are illustrated in the theoretical derivation. Compared to the state-of-the-art method, the proposed method directly works in the state domain, is suitable for any positioning model based on the Kalman filter, and detects the slowly growing fault earlier. The experimental results indicate that the slowly growing fault detection performance of the snapshot integrity algorithms such as RCTM and SRCTM is poor, and SRAIME can detect slowly growing faults earlier than AIME. Meanwhile, SRAIME can be applied to both SPP and PPP, while AIME is only suitable for simulation-based fault detection, not for real-time fault detection.

Acknowledgements

The authors would like to thank Cox Duncan B and Chen Kai for their open source programs in experiments.

Author contributions

ZY: substantial contributions to the conception; the acquisition, analysis, interpretation of data; have drafted the work or substantively revised it. QZ: substantial contributions to the conception; the acquisition, analysis, interpretation of data; have drafted the work or substantively revised it. SZ: the acquisition, analysis, interpretation of data; have drafted the work or substantively revised it. NZ: the acquisition, analysis, interpretation of data; have drafted the work or substantively revised it. KL: the acquisition, analysis, interpretation of data. All authors read and approved the manuscript.

Funding

This work was supported by the Fundamental Research Funds for the Central Universities (No.2019XKQYMS52) and the Priority Academic Program Development of Jiangsu Higher Education Institutions (PAPD).

Availability of data and materials

The datasets used and/or analysed during the current study are available from the corresponding author on reasonable request.

Declarations

Competing interests

We declare that we have no financial and personal relationships with other people or organizations that can inappropriately influence our work. There is no professional or other personal interest of any nature or kind in any product, service and/or company that could be construed as influencing the position presented in, or the review of, the manuscript entitled, "A State-Domain Robust Autonomous Integrity Monitoring by Extrapolation Method for Single Receiver Positioning in the Presence of Slowly Growing Fault."

Received: 19 January 2023 Accepted: 18 May 2023
Published online: 05 July 2023

References

Bhatti, U. I., Ochieng, W. Y., & Feng, S. (2007a). Integrity of an integrated GPS/INS system in the presence of slowly growing errors. Part I: A critical review. *GPS Solutions, 11*, 173–181.

Bhatti, U. I., Ochieng, W. Y., & Feng, S. (2007b). Integrity of an integrated GPS/INS system in the presence of slowly growing errors. Part II: Analysis. *GPS Solutions, 11*, 183–192.

Bhatti, U. I., Ochieng, W. Y., & Feng, S. (2012). Performance of rate detector algorithms for an integrated GPS/INS system in the presence of slowly growing error. *GPS Solutions, 16*, 293–301.

Bruggemann, T. S., Greer, D. G., & Walker, R. A. (2011). GPS fault detection with IMU and aircraft dynamics. *IEEE Transactions on Aerospace and Electronic Systems, 47*(1), 305–316.

Bu, J., Yu, K., Qian, N., Zuo, X., & Chang, J. (2020). Performance assessment of positioning based on multi-frequency multi-GNSS observations: Signal quality, PPP and baseline solution. *IEEE Access, 9*, 5845–5861.

Chen, C., & Kia, S. S. (2021a). A Renyi divergence based approach to fault detection and exclusion for tightly coupled GNSS/INS system. In *Proceedings of the 2021a International Technical Meeting of the Institute of Navigation* (pp. 674–687).

Chen, K., Chang, G., & Chen, C. (2021b). GINav: A MATLAB-based software for the data processing and analysis of a GNSS/INS integrated navigation system. *GPS Solutions, 25*(3), 108.

Cox, D. B. (1978). Integration of GPS with inertial navigation systems (Miscellaneous Topics). *NAVIGATION: Journal of the Institute of Navigation, 25*(2), 236–245.

Diesel, J., & King, J. (1995). Integration of navigation systems for fault detection, exclusion, and integrity determination-Without WAAS. In *Proceedings of the 1995 National Technical Meeting of The Institute of Navigation* (pp. 683–692).

Du, Y., Wang, J., Rizos, C., & El-Mowafy, A. (2021). Vulnerabilities and integrity of precise point positioning for intelligent transport systems: Overview and analysis. *Satellite Navigation, 2*(1), 1–22.

Duník, J., & Straka, O. (2018). State estimate consistency monitoring in Gaussian filtering framework. *Signal Processing, 148*, 145–156.

Gaglione, S., Angrisano, A., Freda, P., Innac, A., Vultaggio, M., & Crocetto, N. (2015). Benefit of GNSS multiconstellation in position and velocity domain. In *2015 IEEE Metrology for Aerospace (MetroAeroSpace)* (pp. 9–14). IEEE.

Gao, Y., Li, Z., & McLellan, J. F. (1997). Carrier phase based regional area differential GPS for decimeter-level positioning and navigation. In *Proceedings of the 10th international technical meeting of the satellite division of the institute of navigation (ION GPS 1997)* (pp. 1305–1313).

Gao, Y., Gao, Y., Liu, B., & Jiang, Y. (2021). Enhanced fault detection and exclusion based on Kalman filter with colored measurement noise and application to RTK. *GPS Solutions, 25*, 1–13.

Geng, Y., & Wang, J. (2008). Adaptive estimation of multiple fading factors in Kalman filter for navigation applications. *GPS Solutions, 12*, 273–279.

Hide, C., Moore, T., & Smith, M. (2003). Adaptive Kalman filtering for low-cost INS/GPS. *The Journal of Navigation, 56*(1), 143–152.

Li, Y., & Cai, C. (2022). A mixed single-and dual-frequency quad-constellation GNSS precise point positioning approach on Xiaomi Mi8 smartphones. *The Journal of Navigation, 75*(4), 849–863.

Li, X., Huang, J., Li, X., Shen, Z., Han, J., Li, L., & Wang, B. (2022a). Review of PPP–RTK: Achievements, challenges, and opportunities. *Satellite Navigation, 3*(1), 28.

Li, X., Wang, B., Li, X., Huang, J., Lyu, H., & Han, X. (2022b). Principle and performance of multi-frequency and multi-GNSS PPP-RTK. *Satellite Navigation, 3*(1), 7.

Li, Z., Wang, L., Wang, N., Li, R., & Liu, A. (2022c). Real-time GNSS precise point positioning with smartphones for vehicle navigation. *Satellite Navigation, 3*(1), 19.

Liu, Y., Xu, X., Liu, X., Zhang, T., Li, Y., Yao, Y., Yi-qing, Y., Liang, W., & Tong, J. (2016). A fast gradual fault detection method for underwater integrated navigation systems. *The Journal of Navigation, 69*(1), 93–112.

Lv, J., Gao, Z., Kan, J., Lan, R., Li, Y., Lou, Y., Yang, H., & Peng, J. (2022). Modeling and assessment of multi-frequency GPS/BDS-2/BDS-3 kinematic precise point positioning based on vehicle-borne data. *Measurement, 189*, 110453.

Paziewski, J. (2022). Multi-constellation single-frequency ionospheric-free precise point positioning with low-cost receivers. *GPS Solutions, 26*(1), 23.

Sanz, J., Juan, J., & Hernández-Pajares, M. (2013). GNSS data processing, Vol. I: Fundamentals and algorithms. *ESA Communications, 14*, 15.

Shinghal, G., & Bisnath, S. (2021). Conditioning and PPP processing of smartphone GNSS measurements in realistic environments. *Satellite Navigation, 2*, 1–17.

Wang, J. G. (2008). Test statistics in Kalman filtering. *Positioning, 7*, 81–90.

Wang, J. G. (2009). Reliability analysis in Kalman filtering. *Journal of Global Positioning Systems, 8*(1), 101–111.

Wang, Y., & Shen, J. (2020). Real-time integrity monitoring for a wide area precise positioning system. *Satellite Navigation, 1*(1), 1–10.

Wanninger, L. (1995). Improved ambiguity resolution by regional differential modelling of the ionosphere. In *Proceedings of the 8th international technical meeting of the satellite division of the institute of navigation (ION GPS 1995)* (pp. 55–62).

Yu, Z., Zhang, Q., Yu, K., & Zheng, N. (2021). A state-domain robust chi-square test method for GNSS/INS integrated navigation. *Journal of Sensors, 2021*, 1–8.

Zhu, Y., Cheng, X., & Wang, L. (2016). A novel fault detection method for an integrated navigation system using Gaussian process regression. *The Journal of Navigation, 69*(4), 905–919.

Zumberge, J. F., Heflin, M. B., Jefferson, D. C., Watkins, M. M., & Webb, F. H. (1997). Precise point positioning for the efficient and robust analysis of GPS data from large networks. *Journal of Geophysical Research: Solid Earth, 102*(B3), 5005–5017.

Publisher's Note